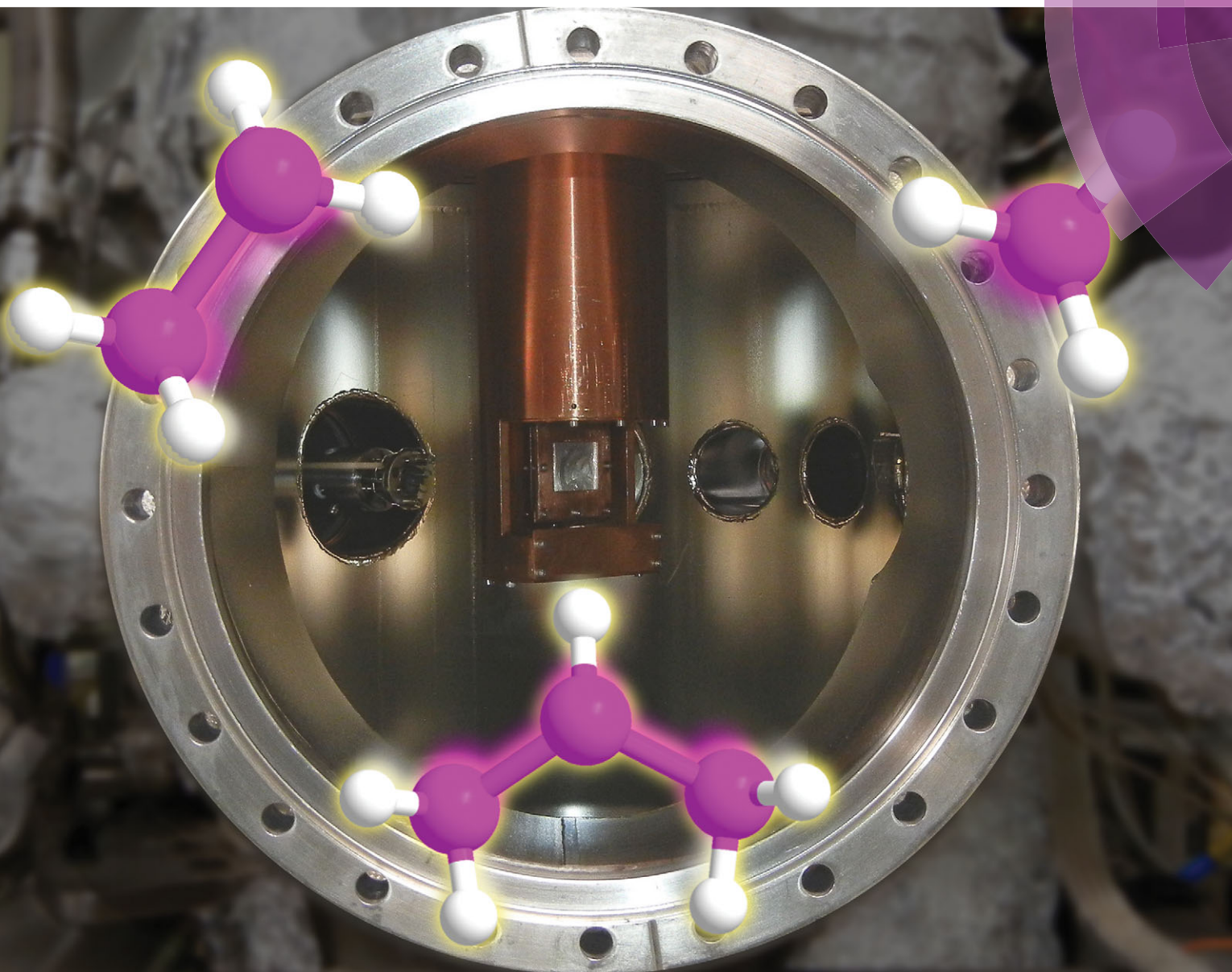


PCCP

Physical Chemistry Chemical Physics

www.rsc.org/pccp



ISSN 1463-9076



PAPER

Agnes H. H. Chang, Ralf I. Kaiser *et al.*

A photoionization mass spectroscopic study on the formation of phosphanes in low temperature phosphine ices



Cite this: *Phys. Chem. Chem. Phys.*,
2015, 17, 27281

A photoionization mass spectroscopic study on the formation of phosphanes in low temperature phosphine ices†

Andrew M. Turner,^a Matthew J. Abplanalp,^a Si Y. Chen,^b Yu T. Chen,^b
Agnes H. H. Chang^{*b} and Ralf I. Kaiser^{*a}

Isovalency rationalizes fundamental chemical properties of elements in the same group, but often fails to account for differences in the molecular structure due to the distinct atomic sizes and electron-pair repulsion of the isovalent atoms. With respect to main group V, saturated hydrides of nitrogen are limited to ammonia (NH₃) and hydrazine (N₂H₄) along with ionic and/or metal-bound triazene (N₃H₅) and potentially tetrazene (N₄H₆). Here, we present a novel approach for synthesizing and detecting phosphanes formed *via* non-classical synthesis exploiting irradiation of phosphine ices with energetic electrons, subliming the newly formed phosphanes *via* fractionated sublimation, and detecting these species *via* reflectron time-of-flight mass spectrometry (ReTOF) coupled with vacuum ultraviolet (VUV) single photon ionization. This approach is able to synthesize, to separate, and to detect phosphanes as large as octaphosphane (P₈H₁₀), which far out-performs the traditional analytical tools of infrared spectroscopy and residual gas analysis *via* mass spectrometry coupled with electron impact ionization that could barely detect triphosphane (P₃H₅) thus providing an unconventional tool to prepare complex inorganic compounds such as a homologues series of phosphanes, which are difficult to synthesize *via* classical synthetic methods.

Received 16th May 2015,
Accepted 21st July 2015

DOI: 10.1039/c5cp02835c

www.rsc.org/pccp

1. Introduction

Ever since Langmuir devised the concept of isovalency in 1919,¹ this framework has presented a fundamental pillar of chemistry and elucidates the periodic property that elements in the same group with an identical valence electron configuration hold similar chemical properties. Isovalency has been exploited to understand the chemical formulas, reaction mechanisms, and even molecular geometries for a vast array of chemical compounds. For instance, the molecular formulas for hydrides of main group V elements – ammonia (NH₃), phosphine (PH₃), arsine (AsH₃), stibine (SbH₃), and bismuthine (BiH₃) – can be rationalized by the ns^2np^3 valence electron configuration of the central atoms. However, factors related to the atomic radius as well as bonding and non-bonding atomic orbitals have shown to result in distinct molecular structures.^{2,3} These differences are most evident considering the elemental forms of the first

two members of main group V: nitrogen and phosphorus. Molecular nitrogen exists as a diatomic molecule (N₂) in the gas phase, while white phosphorus is composed of P₄ tetrahedrons occurring in the liquid and gas phase and exists in equilibrium with diatomic phosphorus (P₂) at elevated temperatures above 1070 K.⁴ An evaluation of the molecular structures of the hydrides of nitrogen and phosphorus demonstrates simultaneously the validity, but also the shortcomings of the isovalency concept.

The two simplest azanes (N_nH_{n+2}; $n = 1, 2$) and phosphanes (P_nH_{n+2}; $n = 1, 2$) have been known for more than a century. The molecular formula of the most common and least toxic azane – ammonia (NH₃) – was determined in 1785⁵ with phosphine (PH₃) being discovered in that same year.⁶ These were followed by diphosphine (P₂H₄) in 1844,⁷ which was surprisingly discovered 50 years before its nitrogen analogue, hydrazine (N₂H₄).⁸ More complex molecules have proven to be more difficult to synthesize. Triazane (N₃H₅) was first reported as a silver-complex⁹ and later monitored *via* its molecular ion exploiting microwave plasma discharge of hydrazine.¹⁰ This study tentatively characterized tetrazane (N₄H₆), but only as a complex with lithium. Thus, free azanes heavier than hydrazine have been difficult to synthesize and require a metal-cation complex to stabilize the molecule in the gas phase or in zeolites.

^a Department of Chemistry, University of Hawaii at Manoa, Honolulu, Hawaii 96822, USA. E-mail: ralfk@hawaii.edu; Tel: +1-808-956-5731

^b Department of Chemistry, National Dong Hwa University, Shoufeng, Hualien 974, Taiwan. E-mail: hhchang@mail.ndhu.edu.tw

† Electronic supplementary information (ESI) available: Calculations and diagrams used to determine the refractive index of phosphine, the experimental ice thickness, and integrated absorption coefficients. See DOI: 10.1039/c5cp02835c

Despite the isovalency between nitrogen and phosphorus, far larger hydrides of phosphorus have been detected.¹¹ Triphosphane (P_3H_5) was first probed *via* Raman spectroscopy as a transient species¹² and was also isolated for preparative studies.¹³ Heated mixtures of diphosphine (P_2H_4) and triphosphane (P_3H_5) produced traces of tetraphosphane (P_4H_6), which could not be purified due to rapid disproportionation. Further heating lead to the formation of poorly defined mixtures of pentaphosphane (P_5H_7), hexaphosphane (P_6H_8), and heptaphosphane (P_7H_9), which could not be separated due to the thermal instability of higher phosphanes. Octaphosphane (P_8H_{10}) and nonaphosphane (P_9H_{11}) were only identified tentatively.¹¹ The fact that phosphorus can form more complex hydrides than nitrogen illustrates that additional factors beyond isoelectronicity affect the chemistry of these elements, such as the established tendency of nitrogen to favor the formation of multiple bonds due to the smaller radius of the nitrogen atom (71 pm) compared to phosphorus (109 pm).¹⁴ However, despite the tentative identification of higher phosphanes, their underlying synthetic pathways together with their explicit isolation and protocols to their clean preparation have not been established to date.

Here, we demonstrate that phosphanes up to octaphosphane (P_8H_{10}) can be efficiently prepared and thereafter separated *via* fractionated sublimation upon exposure of phosphine ices to energetic electrons at ultralow temperatures of 5.5 K. The low

temperature was chosen to minimize thermal chemistry in the ice. Reflectron time-of-flight (ReTOF) mass spectroscopy coupled with 'soft' single vacuum ultraviolet (VUV) photon ionization at 10.49 eV is applied to explicitly identify the molecular formulas of the newly synthesized phosphanes on line and *in situ* upon their sublimation into the gas phase upon warming of the irradiated

Table 1 Infrared absorption assignments for phosphine ice at 5.5 K and the products of electron irradiation

Assignment ^a	Position (cm^{-1})
Phosphine ice, pre-irradiation (5.5 K)	
ν_2 (δ (HPP))	983
ν_4 (δ (HPP))	1097, 1108sh
$\nu_2 + \nu_4$	2067, 2083
$2\nu_4$	2195
ν_1 (ν (PH))	2303
ν_3 (ν (PH))	2316
$\nu_1/\nu_3 + \nu_L$	2376, 2426, 2461
$3\nu_2$	2905
$\nu_1 + \nu_2$	3288
$\nu_1 + \nu_4$	3392
$\nu_3 + \nu_4$	3405
$2\nu_1$	4536
$\nu_1 + \nu_3$	4621
New peaks from irradiation	
P_2H_4 (ν_{11} , δ (HPP))	1061
P_2H_4 (ν_5 , ν (PH))	2294
P_3H_5 (ν (PH))	2264, 2288
P_3H_5 (δ (HPP))	1059

^a Assignments based on previous studies.^{43,44}

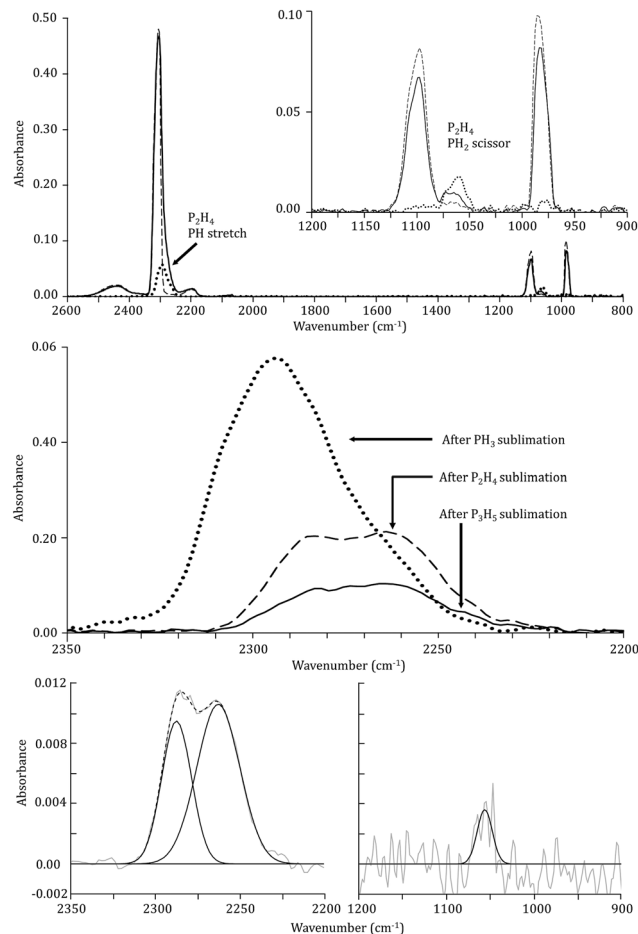


Fig. 2 (Top) Overlay of infrared spectra of solid PH_3 taken before (dashed line) and after (solid line) irradiation, with the spectrum after PH_3 sublimated (85 K, dotted line) emphasizing the products of irradiation. The inset expands the lower intensity region from 1200–900 cm^{-1} . (Center) Infrared spectra of the P–H stretching region after PH_3 (85 K, dotted line), P_2H_4 (130 K, dashed line), and P_3H_5 (165 K, solid line) sublime. (Bottom) Infrared spectrum of P_3H_5 obtained by subtracting the post- P_3H_5 sublimation spectrum from its pre-sublimation spectrum. The peaks at 2264 cm^{-1} and 2288 cm^{-1} (left) result from P–H stretching while the peak at 1059 cm^{-1} (right) corresponds to H–P–P bending.

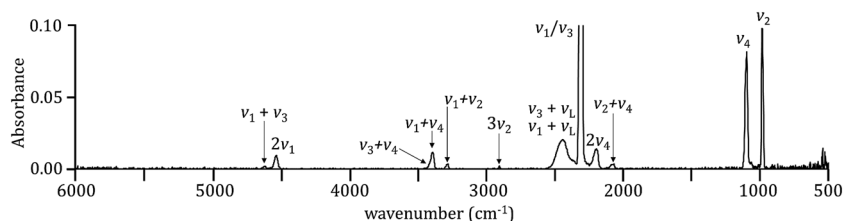


Fig. 1 Infrared spectrum of pre-irradiated solid phosphine taken at 5.5 K.

target to 300 K. Our study presents clear evidence of higher molecular mass phosphanes thus providing a clean route to their formation up to octaphosphane (P_8H_{10}) *via* exposure of phosphine ices to energetic electrons followed by fractionated sublimation of the phosphanes. This study further provides a proof of concept for a novel adaptation of ReTOF mass spectroscopy coupled with VUV single-photon ionization to form and to identify inorganic molecules, which are difficult to synthesize *via* classical synthetic methods.

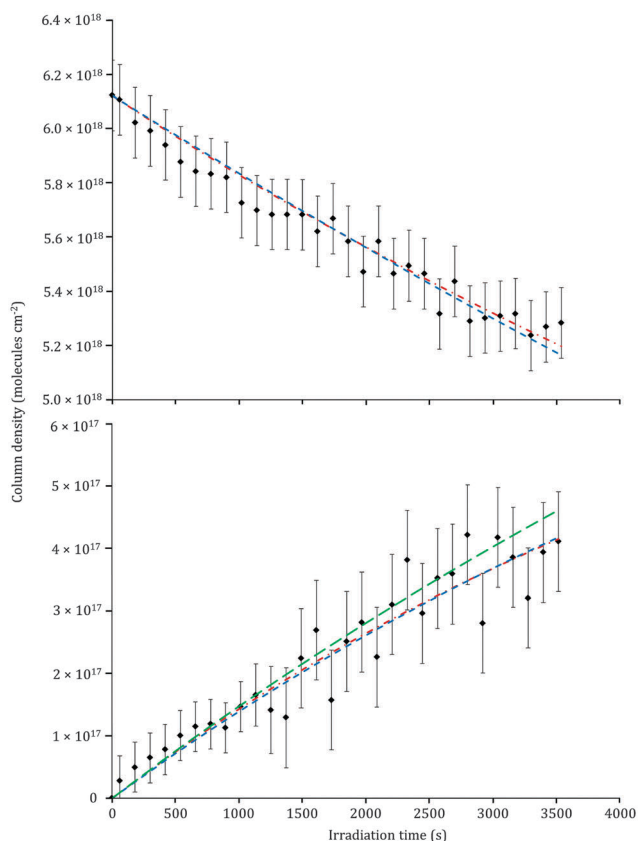


Fig. 3 Temporal profiles of the decay of PH_3 (top) and production of P_2H_4 (bottom) during irradiation. The intensity of the PH_3 ν_2 vibrational mode at 983 cm^{-1} was used as a proxy for the abundance of PH_3 while the P_2H_4 ν_{11} vibrational mode at 1061 cm^{-1} was used to monitor P_2H_4 . Fits to the second-order reaction of $2PH_3 \rightarrow P_2H_4 + H_2$ (red) along with the first-order reaction $(PH_3)_2 \rightarrow P_2H_4 + H_2$ (blue) are shown coupled with the reaction $P_2H_4 \rightarrow$ products. The green line indicates the total amount of P_2H_4 formed from PH_3 decay with the assumption that P_2H_4 does not further react.

Table 2 Rate constants for reactions of PH_3 and P_2H_4

Reaction	Reaction order	k
$(PH_3)_2 \rightarrow P_2H_4 + 2H/H_2$	1	$4.8 \pm 0.1 \times 10^{-5b}$
$P_2H_4 \rightarrow$ products	1	$8 \pm 3 \times 10^{-5b}$
$2PH_3 \rightarrow P_2H_4 + 2H/H_2$	2	$8.2 \pm 0.1 \times 10^{-24a}$
$P_2H_4 \rightarrow$ products	1	$6 \pm 2 \times 10^{-5b}$

^a Units $\text{cm}^2\text{ molecules}^{-1}\text{ s}^{-1}$. ^b Units s^{-1} .

2. Experimental section

The experiments were conducted in a contamination-free ultra-high vacuum stainless steel chamber evacuated to a few 10^{-11} Torr using oil-free turbomolecular pumps and dry scroll backing pumps, which has been described previously.^{15–24} Briefly, a silver mirror substrate is mounted onto a rotatable cold finger made of oxygen-free high-conductivity copper (OFHC) cooled to $5.5\text{ K} \pm 0.1$ by a closed-cycle helium refrigerator (Sumitomo Heavy Industries, RDK-415E). Phosphine (Sigma-Aldrich, 99.9995%) was condensed on the substrate through a glass capillary at a pressure of 5×10^{-8} Torr at thicknesses of $920 \pm 20\text{ nm}^{25–27}$ (ESI[†]).

Table 3 Observed masses from the reflectron time-of-flight mass spectrometer

Mass	Formula	Comments	Parent compound
31	P^+	Fragment	PH_3
32	PH^+	Fragment	PH_3
33	PH_2^+	Fragment	PH_3
34	PH_3^+	Parent	PH_3
35	PH_2D^+	Isotope	PH_3
	PH_4^+	Protonated parent	
	PH_4^+	Fragment	P_3H_5, P_4H_6
64	$P_2H_2^+$	Fragment	P_3H_5
65	$P_2H_3^+$	Fragment	P_3H_5
66	$P_2H_4^+$	Parent	P_2H_4
67	$P_2H_3D^+$	Isotope	P_2H_4
	$P_2H_5^+$	Protonated parent	
	$P_2H_5^+$	Fragment	P_4H_6, P_5H_7
96	$P_3H_3^+$	Fragment	P_4H_6
97	$P_3H_4^+$	Fragment	P_4H_6
98	$P_3H_5^+$	Parent	P_3H_5
99	$P_3H_4D^+$	Isotope	P_3H_5
	$P_3H_6^+$	Protonated parent	
	$P_3H_6^+$	Fragment	P_6H_8
126	$P_4H_2^+$	Fragment	P_6H_8
127	$P_4H_3^+$	Fragment	P_6H_8
128	$P_4H_4^+$	Fragment	P_5H_7
129	$P_4H_5^+$	Fragment	P_5H_7
130	$P_4H_6^+$	Parent	P_4H_6
159	$P_5H_4^+$	Fragment	P_7H_9
160	$P_5H_5^+$	Fragment	P_6H_8, P_7H_9
161	$P_5H_6^+$	Fragment	P_6H_8
162	$P_5H_7^+$	Parent	P_3H_7
191	$P_6H_5^+$	Fragment	P_7H_9, P_8H_{10}
193	$P_6H_7^+$	Fragment	P_7H_9
223	$P_7H_6^+$	Fragment	P_8H_{10}
225	$P_7H_8^+$	Fragment	P_8H_{10}

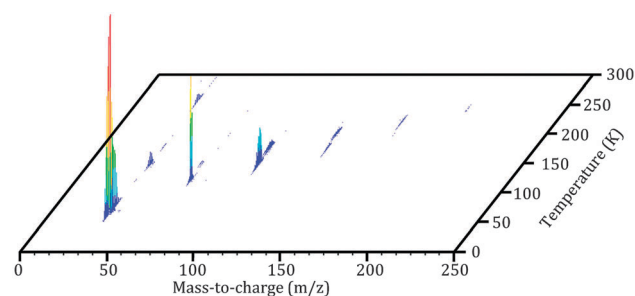


Fig. 4 ReTOF mass spectrometry data as a function of sublimation temperature as irradiated phosphine ice was heated from 5.5 K to 300 K at 1 K min^{-1} .

The refractive index (n_{PH_3}) of solid phosphine necessary to calculate the thickness was experimentally determined exploiting laser

interferometry by two helium–neon lasers²⁸ to be $n_{\text{PH}_3} = 1.51 \pm 0.04$. The ices were isothermally irradiated with 5 keV electrons

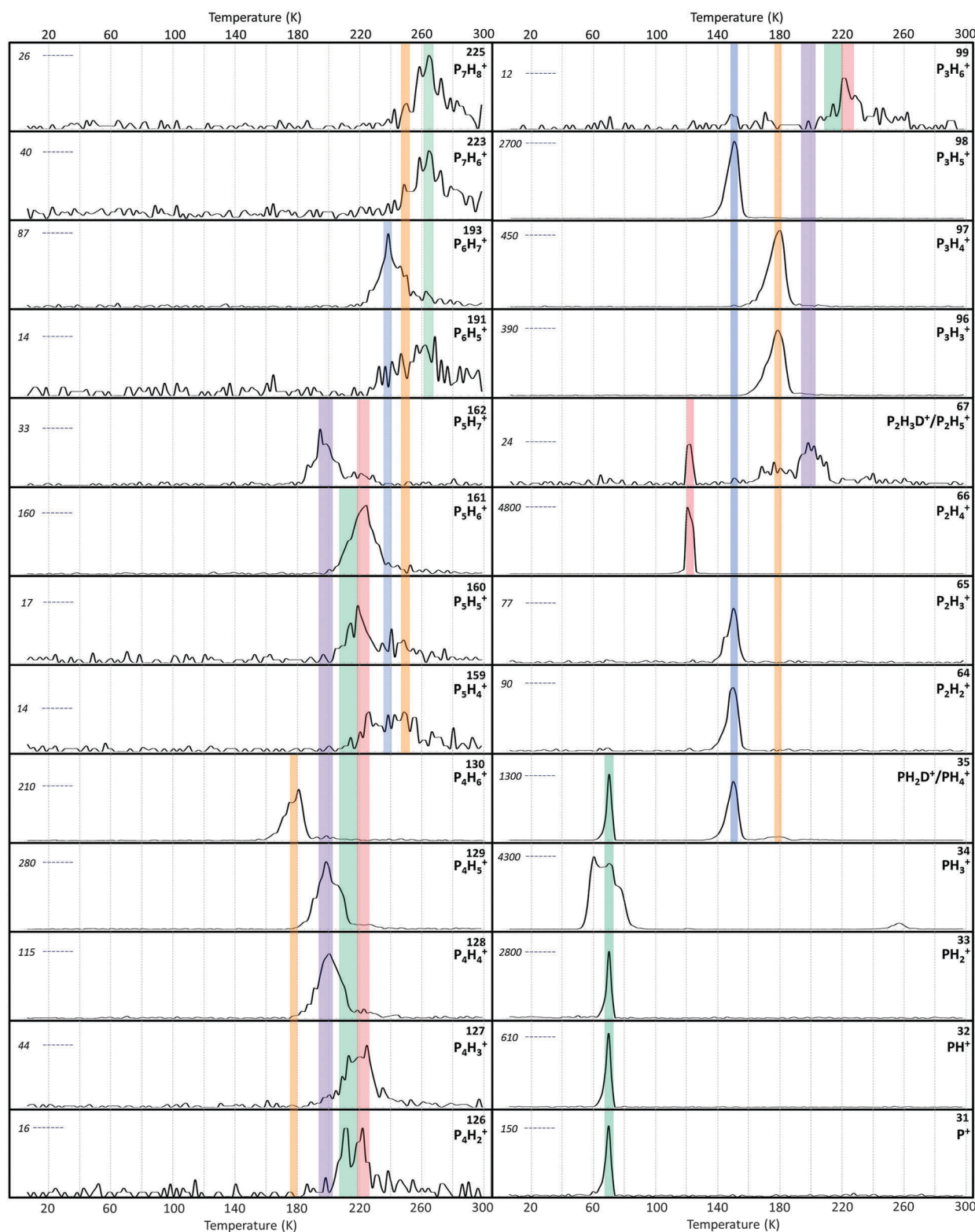


Fig. 5 ReTOF data as a function of temperature for the indicated masses (top-right in bold with formula). The irradiated phosphine sample was heated from 5.5 K to 300 K at 1 K min^{-1} . The strongest peak intensity is shown on the left in italics, and colored lines trace sublimation events that occur at the same temperature. The peak shape of phosphine ($m/z = 34$) results from detector saturation.

at fluxes as high as 2×10^{10} electrons $\text{s}^{-1} \text{cm}^{-2}$ over an area of $1.0 \pm 0.1 \text{ cm}^2$ at an angle of incidence of 70° relative to the substrate normal. The average absorbed dose per target molecule was determined from Monte Carlo (CASINO)²⁹ simulations using the density of 0.90 g cm^{-3} for solid phosphine³⁰ to be $0.17 \pm 0.04 \text{ eV}$ per molecule. The ices were monitored on line and *in situ* during the irradiation using a Fourier Transform Infrared Spectrometer (FTIR, Nicolet 6700) over a range of 6000 cm^{-1} to 500 cm^{-1} at 4 cm^{-1} resolution. One hour after the irradiation, a temperature programmed desorption (TPD) protocol heated the irradiated ices to 300 K at rates of 1 K min^{-1} . During the sublimation, the molecules were probed *via* reflectron time-of-flight mass spectrometry (Jordan TOF Products, Inc.) after photoionization (ReTOFMS-PI) at 118.2 nm (10.49 eV).¹⁵ Here, the pulsed (30 Hz) coherent vacuum ultraviolet (VUV) light was generated *via* four wave mixing using xenon (99.999%) as a non-linear medium. The third harmonic (354.6 nm) of a high-power pulsed neodymium-doped yttrium aluminum garnet laser (Nd:YAG, Spectra Physics, PRO-250, 30 Hz) underwent a frequency tripling process ($\omega_{\text{VUV}} = 3\omega_1$) to obtain the 118.2 nm photons at levels of $\sim 10^{14}$ VUV photons per pulse.²⁰ The xenon was pulsed into an evacuated mixing chamber at an operating pressure of $3 \times 10^{-4} \text{ Torr}$. The VUV light was separated from the fundamental using a lithium fluoride (LiF) plano-convex lens³¹ (ISP Optics, LF-PX-38-150) based on distinct refractive indices of the lens material for different wavelengths and then directed 1 mm above the ice surface.²⁰ The photoionized molecules were then directed toward the focusing regions by a repeller plate (held at ground) and an extraction plate (-190 V) with the field between the repeller and extraction plates held at a voltage of -210 V . Mass-to-charge ratios were determined based on the arrival time of the ions at a multichannel plate; the signal was amplified with a fast preamplifier (Ortec 9305) and recorded

using a bin width of 4 ns, which was triggered at 30 Hz (Quantum Composers, 9518).

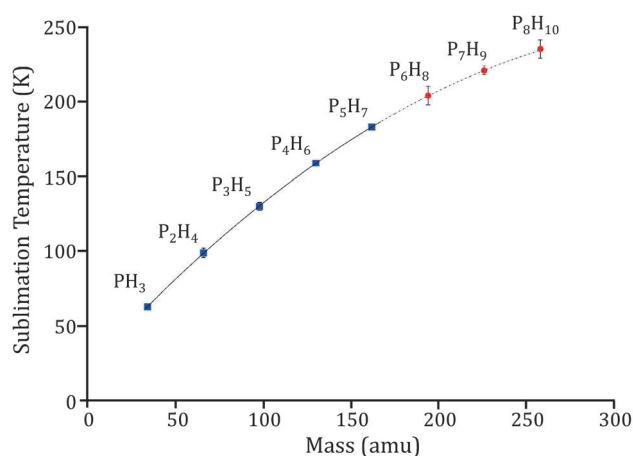


Fig. 6 Sublimation temperatures as a function of mass observed using the ReTOF mass spectrometer. Blue squares represent phosphanes that were directly observed, while red circles represent phosphanes that were indirectly identified from predicted mass fragments. The five observed phosphanes were used to create the solid trend line, while the dashed line shows the projection of this trend line at higher masses.

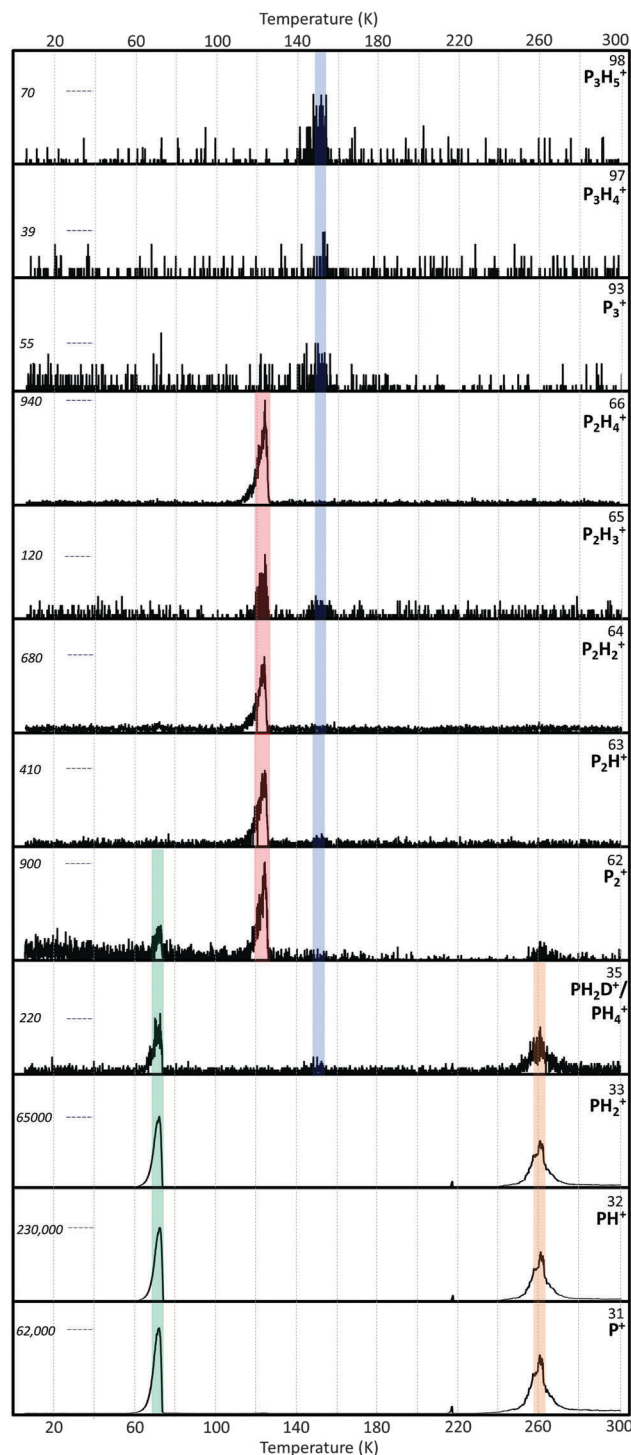


Fig. 7 Residual gas analysis data (quadrupole mass spectrometry) plotted as a function of temperature for the indicated masses (top-right in bold with formula). The irradiated phosphine sample was heated from 5.5 K to 300 K at 1 K min^{-1} . The strongest peak intensity is shown on the left in italics, and colored lines trace sublimation events that occur at the same temperature. Molecular phosphine ($m/z = 34$) was not measured due to saturation concerns.

3. Theoretical methods

The structural isomers and adiabatic ionization energies from PH_3 to P_8H_{10} were investigated with *ab initio* electronic structure calculations. The optimized geometries and harmonic frequencies of the neutral and ionic species were obtained with the hybrid density functional theory, B3LYP/cc-pVTZ.^{32–35} Their energies were refined further by utilizing the CCSD(T)/cc-pVTZ with B3LYP/cc-pVTZ zero-point energy corrections.^{36–39} The adiabatic ionization energy of each species was then computed by taking the energy difference between the neutral and ionic counterparts; this procedure reproduced the ionization energies within ± 0.1 eV.^{40,41} The GAUSSIAN 09 program was employed for the electronic structure calculations.⁴²

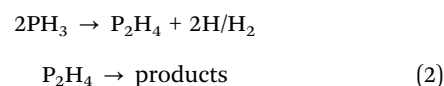
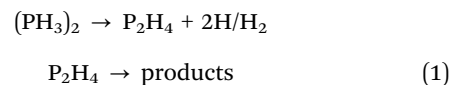
4. Results and discussion

4.1. Infrared spectroscopy

4.1.1. Qualitative analysis. During the irradiation, new absorption features emerged (Table 1, Fig. 1 and 2). The absorptions at 1061 cm^{-1} and at 2294 cm^{-1} , which are easily recognizable in the post-irradiation infrared spectrum recorded at 5.5 K, could be assigned to diphosphine (P_2H_4) (Fig. 2 top); these data agree very well with previous literature data at 1052 cm^{-1} and 2299 cm^{-1} .⁴³ No additional new absorption features were observable at 5.5 K. Upon annealing the irradiated ices to 85 K, the phosphine ice (PH_3) fully sublimed, and the 1061 cm^{-1} and at 2294 cm^{-1} absorptions attributed to diphosphine (P_2H_4) became easily identifiable (Fig. 2 center). Upon annealing to 130 K, diphosphine (P_2H_4) sublimed completely, and absorption features of triphosphane (P_3H_5) emerged at 1059 cm^{-1} (H–P–P bending), 2264 cm^{-1} (P–H stretching), and 2288 cm^{-1} (P–H stretching) (Fig. 2 bottom).⁴⁴ After the sublimation of triphosphane (P_3H_5) at 165 K, a broad absorption from 2310 cm^{-1} to 2280 cm^{-1} characteristic of the P–H stretching in higher phosphanes remains. These spectra demonstrate the limitations of distinguishing higher molecular weight phosphanes exploiting infrared spectroscopy since the most intense absorption of all phosphanes – the P–H stretching mode – occurs over a narrow spectral range. For the remainder of the heating process, these absorptions slowly decayed into the baseline and disappeared near 300 K.

4.1.2. Quantitative analysis – reaction pathways. Having assigned the absorptions first qualitatively, we are now attempting to elucidate the underlying decomposition (reactant) and formation pathways of the product(s). For this, we traced the temporal profiles of the phosphine reactant and also of the deconvoluted bands of the products during the irradiation (Fig. 3) and utilized a set of coupled differential equations to numerically fit these temporal profiles, *i.e.* the column density of the reactant/product(s) *versus* the irradiation time. To determine the column density of phosphine, the ν_2 fundamental at 983 cm^{-1} was exploited since the ν_1 and ν_3 modes overlap with the P–H stretching modes of the reaction product(s) (ESI^\dagger). The ν_{11} fundamental at 1061 cm^{-1} was used to determine the column density of diphosphine (P_2H_4). Since this mode

overlaps slightly with ν_4 mode of phosphine, the peak areas of the ν_{11} and ν_4 modes were determined by deconvoluting the spectra.⁴⁵ Two reaction schemes were explored to fit the column densities with the resulting rate constants listed in Table 2. Eqn (1) proposes a first order decay of phosphine dimers (PH_3)₂ in the condensed phase leading to diphosphine (P_2H_4) plus atomic/molecular hydrogen followed by the subsequent reaction of diphosphine (P_2H_4) to higher order phosphanes. Eqn (2) probes the decomposition of second order decay of phosphine (PH_3) to diphosphine (P_2H_4) plus atomic/molecular hydrogen followed once again by the transformation of diphosphine (P_2H_4) to higher order phosphanes.



The results as compiled in Table 3 show that both reaction schemes fit the decay of phosphine (PH_3) and the rise profile of diphosphine (P_2H_4) equally well. Note that it was important to include a reaction pathway from diphosphine (P_2H_4) to higher order phosphanes to avoid an overproduction of diphosphine (P_2H_4) at longer irradiation times.

4.1.3. Quantitative analysis – mass balance. Considering the infrared absorption coefficients of $5.1 \pm 0.3 \times 10^{-19}\text{ cm molecule}^{-1}$ for the ν_2 band (983 cm^{-1}) for phosphine and of $7.0 \pm 0.4 \times 10^{-19}\text{ cm molecule}^{-1}$ for the ν_{11} band (1061 cm^{-1}) for diphosphine (P_2H_4) (ESI^\dagger), $9.4 \pm 0.6 \times 10^{17}\text{ molecules cm}^{-2}$ of phosphine and $4.6 \pm 0.3 \times 10^{17}\text{ molecules cm}^{-2}$ of diphosphine were destroyed and produced, respectively, during the electron irradiation. This was derived based on a comparison of the infrared spectra taken before and after the electron irradiation. This leads to a production rate of $9.4 \pm 0.8 \times 10^{-2}\text{ molecules eV}^{-1}$ at 5.5 K and a diphosphine yield of $6.9 \pm 0.6\%$ with respect to phosphine. The formation of diphosphine accounts for $89 \pm 4\%$ of the phosphorus from

Table 4 Observed masses from the residual gas analyzer (QMS)

Mass	Formula	Comments	Parent compound
31	P^+	Fragment	PH_3
32	PH^+	Fragment	PH_3
33	PH_2^+	Fragment	PH_3
35	PH_2D^+	Isotope	PH_3
	PH_4^+	Protonated parent	
	PH_4^+	Fragment	P_3H_5
62	P_2^+	Recombination	PH_3
		Fragment	P_2H_4
63	P_2H^+	Fragment	P_2H_4
64	P_2H_2^+	Fragment	P_2H_4
65	P_2H_3^+	Fragment	P_2H_4 , P_3H_5
66	P_2H_4^+	Parent	P_2H_4
93	P_3^+	Fragment	P_3H_5
97	P_3H_4^+	Fragment	P_3H_5
98	P_3H_5^+	Parent	P_3H_5

the destroyed phosphine reactant. Therefore, $11 \pm 4\%$ of the phosphine has to be converted to hitherto unidentified higher order phosphanes containing more than two phosphorus atoms. The formation of higher phosphanes is also in line with a destruction pathway of diphosphine to higher phosphanes required to avoid an overproduction of diphosphine at longer irradiation times (Section 4.1.2).

4.2. Reflectron time-of-flight mass spectroscopy (ReTOF)

Despite the FTIR spectra, with the exception of diphosphine (P_2H_4), these data alone cannot identify individual higher phosphanes because the group frequencies, for instance of

the P–H stretches and bending modes, overlap significantly. We thus turned to the complementary, highly sensitive ReTOFMS-PI technique to identify individual phosphanes based on their mass-to-charge ratios and the sublimation temperatures upon annealing of the irradiated ices to 300 K. Fig. 4 depicts the ReTOF mass spectra as a function of temperature during the warm up phase after irradiating the phosphine ices obtained by photoionizing the subliming molecules with 10.49 eV photons. The spectra display the intensity of the ion counts of the photoionized products subliming into the gas phase at well-defined temperatures. Here, ions with mass-to-charge ratios up to $m/z = 225$ are observable. The temperature programmed desorption (TPD) profiles of the

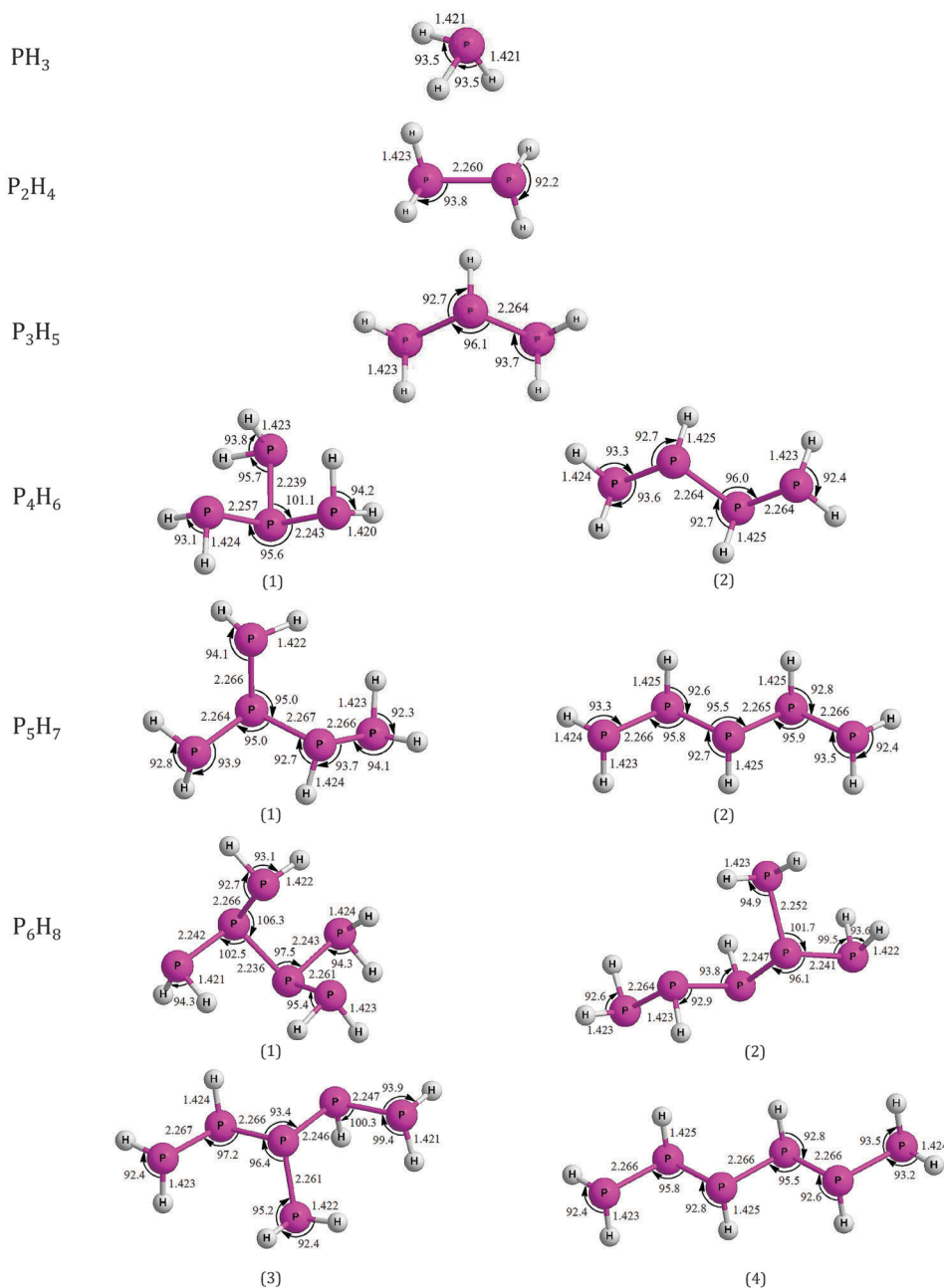


Fig. 8 Calculated bond lengths and angles for isomers of PH_3 through P_6H_8 .

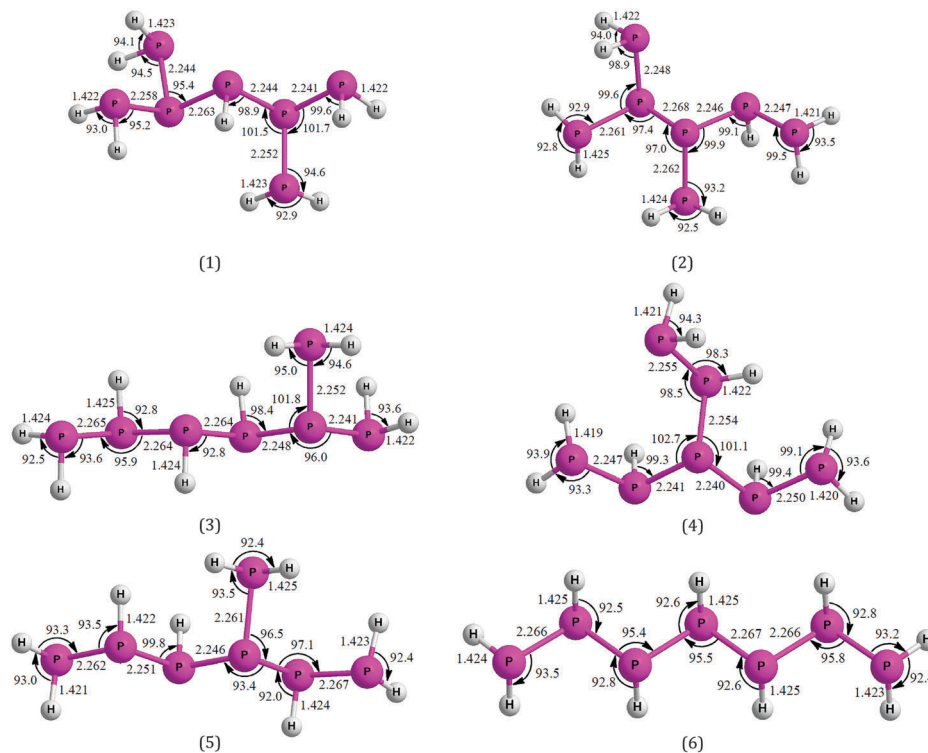


Fig. 9 Calculated bond lengths and angles for isomers of P_7H_9 .

individual ions are compiled in Fig. 5; these TPD spectra are color coded to highlight to what extent ions at lower mass-to-charge ratios originate as fragment ions from corresponding higher mass species. Identical TPD profiles of ions at two distinct mass-to-charge ratios in a well-defined temperature range indicate that both species originate from a common parent and correspond to molecular fragment ions.

As expected from the infrared data, phosphine (PH_3) and diphosphine (P_2H_4) can be identified with the ReTOFMS-PI technique *via* their parent ions at $m/z = 34$ (PH_3^+) and 66 ($P_2H_4^+$) (Fig. 5 and Table 3). Here, phosphine (PH_3) can fragment to $m/z = 33$ (PH_2^+), 32 (PH^+), and 31 (P^+) as well, diphosphine (P_2H_4) does not fragment at all upon 10.49 eV photoionization, and the signal at $m/z = 67$ can originate from $P_2DH_3^+$ and/or $P_2H_5^+$ potentially formed *via* proton transfer from PH_4^+ . Further, higher order phosphanes can be identified. These are triphosphane (P_3H_5) assigned *via* its parent peak at $m/z = 98$ ($P_3H_5^+$) and the fragments at $m/z = 65$ ($P_3H_3^+$), 64 ($P_3H_2^+$), and 35 (PH_4^+). It is important to note that as the molecular mass increases from 34 amu (PH_3) *via* 66 (P_2H_4) to 98 (P_3H_5), the onset of the sublimation also rises from 63 K *via* 99 K to 130 K (Fig. 6). It is notable that beginning with tetraphosphane (P_4H_6), fragmentation of the parent upon photoionization becomes significant; the intensities of the fragment ions are always higher than the respective molecular parent ions. These fragmentation patterns become more pronounced at higher masses. While the singly ionized tetraphosphane (P_4H_6) ($m/z = 130$) holds an abundance of about 50% with respect to the fragments at $m/z = 96$ ($P_3H_3^+$) and 97 ($P_3H_4^+$), the relative abundance of the parent ion of pentaphosphane (P_5H_7) depicts an intensity of only about 10%

compared to their most intense fragments at $m/z = 129$ ($P_4H_5^+$). Beginning with hexaphosphane (P_6H_8), fragmentation occurs to such an extent that the molecular ion can no longer be directly observed. However, the characteristic phosphane fragmentation pattern of PH_2 -loss, which produces the largest fragments of P_5H_7 and P_4H_6 and the second largest fragment, due to slightly more PH_3 -loss fragmentation, of P_3H_5 , continues with fragment ions $m/z = 161$ ($P_5H_6^+$), 193 ($P_6H_7^+$), and 225 ($P_7H_8^+$), which correlate to parent compounds hexaphosphane (P_6H_8), heptaphosphane (P_7H_9), and octaphosphane (P_8H_{10}). Since these larger phosphanes were not directly observed *via* their molecular ions, their fragments' sublimation temperatures were utilized to assign the sublimation temperature of their parent compounds. A regression curve (Fig. 6) for the five phosphanes (PH_3 to P_5H_7) directly observed *via* their molecular parent ions was explored and extrapolated toward higher masses; these predictions depict an excellent agreement with the assigned sublimation temperatures for the high mass phosphanes from P_6H_8 through P_8H_{10} based on their observed fragments.

Since traditional residual gas analyzers are utilized to detect newly synthesized molecules such as phosphanes in the gas phase, we compare the ReTOF data with those obtained by a residual gas analyzer (RGA; quadrupole mass spectrometer) in electron impact mode with 100 eV electrons at an emission current of 1 mA (Fig. 7 and Table 4). The RGA data are consistent, but more limited than the data of the ReTOF mass spectrometer. The only products identified *via* the RGA are diphosphane (P_2H_4) and triphosphane (P_3H_5). Although the parent peak of the latter is tenuous in the RGA, it is notable

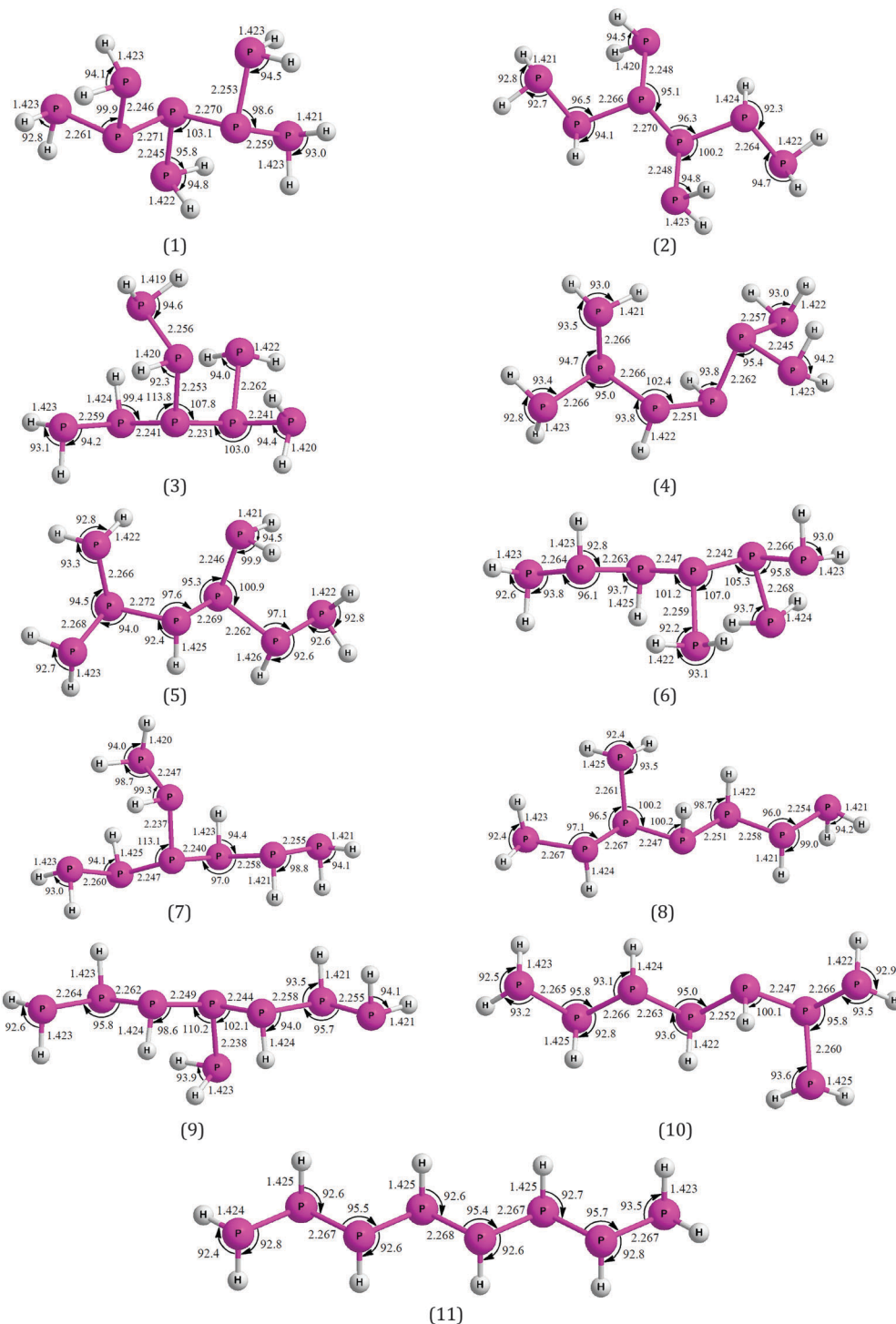


Fig. 10 Calculated bond lengths and angles for isomers of P_8H_{10} .

that the signal for PH_4^+ ($m/z = 35$) occurred as a fragment ion of triphosphane upon ionization in both the RGA and the ReTOF. Therefore, our data demonstrate that a fractionated sublimation of synthesized phosphanes combined with photoionization mass spectrometry presents an ideal, unconventional tool to identify thermally labile molecules, which are difficult to synthesize by classical 'inorganic synthetic approaches'.

4.3 Theoretical calculations

The optimized geometrical structures for distinct phosphanes and their isomers up to octaphosphane (P_8H_{10}) (Fig. 8–10 and Table 5) indicate that the predicted phosphorus–hydrogen (P–H) bond lengths occur only in a narrow range from 142 to 143 pm across all compounds while the phosphorus–phosphorus (P–P) bond lengths vary from 223 to 227 pm with no significant

correlation between the molecular size or primary, secondary, or tertiary phosphorus atoms. The H–P–H bond angles show little variation among molecules holding values from 92° to 95°. Similar values can be seen for the H–P–P bond angles, in particular when the molecule contains no branched moieties. However, in a few cases such as the P₆H₈-2 isomer, all branched P₇H₉ isomers, and several P₈H₁₀ isomers, this bond angle increased to about 100° mainly when the central atom of the H–P–P moiety was a secondary phosphorus atom connected to a tertiary phosphorus. Two additional instances occurred with the central phosphorus attached to a terminal phosphorus atom in the P₈H₁₀ isomers. Besides the bond lengths, it is interesting to investigate trends in the relative stabilities of the isomers. Here, the relative energies of the isomers clearly depicts that branched isomers are energetically preferred compared to the least stable chain isomer, in agreement with previous experimental abundances.¹¹ The relative energy difference between the straight-chain and the most highly branched isomers are 9 kJ mol⁻¹ (P₄H₆), 6 kJ mol⁻¹ (P₅H₇), 16 kJ mol⁻¹ (P₆H₈), 19 kJ mol⁻¹ (P₇H₉), and 29 kJ mol⁻¹ (P₈H₁₀). As evident

Table 5 Calculated ionization energies and relative isomer energies for PH₃ to P₈H₁₀

Isomer ^a	Ionization energy ^b (eV)	Ionization energy ^c (eV)	Ionization energy ^d (eV)	Relative energy (kJ mol ⁻¹)
PH ₃	9.82	9.74	9.87	—
P ₂ H ₄	8.68	8.76	8.8	—
P ₃ H ₅	8.10	8.23	8.7	—
P ₄ H ₆ (1)	7.74	7.89		0
P ₄ H ₆ (2)	7.81	8.00		9
P ₅ H ₇ (1)	7.52	7.71		0
P ₅ H ₇ (2)	7.64	7.87		6
P ₆ H ₈ (1)	7.62	7.76		0
P ₆ H ₈ (2)	7.47	7.68		5
P ₆ H ₈ (3)	7.39	7.60		7
P ₆ H ₈ (4)	7.53	7.79		16
P ₇ H ₉ (1)	7.45	7.69		0
P ₇ H ₉ (2)	7.30	7.52		0.4
P ₇ H ₉ (3)	7.44	7.69		9
P ₇ H ₉ (4)	7.29	7.50		10
P ₇ H ₉ (5)	7.34	7.55		11
P ₇ H ₉ (6)	7.47	7.74		19
P ₈ H ₁₀ (1)	7.24	7.49		0
P ₈ H ₁₀ (2)	7.26	7.50		4
P ₈ H ₁₀ (3)	7.44	7.65		7
P ₈ H ₁₀ (4)	7.36	7.62		11
P ₈ H ₁₀ (5)	7.28	7.55		12
P ₈ H ₁₀ (6)	7.49	7.68		12
P ₈ H ₁₀ (7)	7.57	7.91		15
P ₈ H ₁₀ (8)	7.30	7.50		19
P ₈ H ₁₀ (9)	7.49	7.91		20
P ₈ H ₁₀ (10)	7.38	7.57		21
P ₈ H ₁₀ (11)	7.40	7.69		29

^a The number in parentheses labels the isomer with the lowest energy isomer listed first (Fig. 8–10). ^b B3LYP/cc-pVYZ energy with zero-point correction. ^c CCSD(T)/cc-pVTZ with B3LYP/cc-pVTZ zero-point energy correction. ^d Reference ionization energies.^{46–48}

from Table 5, this energy difference becomes more pronounced for larger molecules. Finally, let us investigate the ionization energies of the phosphanes. Experimentally, the adiabatic ionization energies have only been reported for phosphine (PH₃),⁴⁶ diphosphine (P₂H₄),⁴⁷ and triphosphane (P₃H₅)⁴⁸ to be 9.9 eV, 8.8 eV, and 8.7 eV, respectively. Considering phosphine (PH₃) and diphosphine (P₂H₄), the computed adiabatic ionization energies at the CCSD(T)/cc-pVTZ level of theory are only lower by 0.13 eV and 0.04 eV, respectively. Note that the discrepancy of the computed and experimentally determined adiabatic ionization energy of triphosphane (P₃H₅) could be an artifact of only one experimental characterization, which exploited electron impact mass spectrometry, *i.e.* utilizing a ‘broad’ electron beam with poor resolution. Therefore, we can conclude that the computed ionization energies for are about 0.1 eV lower when compared to the experimental predictions; this shift is in line with previous computations of adiabatic ionization energies of polyacetylenes⁴⁰ and nitrogen-terminated carbon clusters.⁴¹ With respect to higher phosphanes, the calculated ionization energies decrease as the molecules become larger from 7.89 eV to 7.49 eV from tetraphosphane to octaphosphane, respectively. Interestingly, the ionization potentials for a set of isomers are similar to each other without a correlation to branching. The range of CCSD(T)/cc-pVTZ ionization energies are 7.89–8.00 eV (P₄H₆), 7.71–7.87 eV (P₅H₇), 7.60–7.79 eV (P₆H₈), 7.50–7.74 eV (P₇H₉), and 7.49–7.91 eV (P₈H₁₀). The ionization energies show little difference between P₇H₉ and P₈H₁₀ isomers, and this trend is expected to continue with higher-order phosphanes. Most importantly, all ionization energies are well below 10.49 eV – the energy of the VUV photon utilized to photoionize the subliming molecules in the present experiments.

5. Conclusion

An exposure of phosphine (PH₃) ices to energetic electrons produced a homologues series of saturated phosphanes as complex as octaphosphane (P₈H₁₀). This finding is in quite contrast to isoelectronic ammonia (NH₃) systems,^{49–53} leading only to hydrazine (N₂H₄) as the most complex hydrogenated nitrogen compound. Despite the isovalency, similar experimental conditions (temperature, radiation exposure) have been shown to produce far larger hydrides of phosphorus than those of isoelectronic nitrogen. Here, the smaller N–N bond distance (145 pm)⁵⁴ compared to typical P–P bonds (221 pm)⁴³ contributes to the decreased stability of complex nitrogen-based hydrides. The method of vacuum ultraviolet (VUV) single photon ionization to detect inorganic compounds synthesized through non-classical, radiation induced synthetic pathways with the extremely sensitive ReTOFMS-PI technique has proven to be far more illuminating than traditional experiments employing only FTIR and RGA mass spectroscopic analysis to identify complex phosphanes. The latter technique limited the observations to diphosphine (P₂H₄) and triphosphane (P₃H₅), while compounds as large as octaphosphane (P₈H₁₀) could be monitored using ReTOFMS-PI. Future experiments will be designed to identify

individual isomers by selectively photoionizing these isomers with VUV photons exploring four-wave difference and sum mixing^{31,55} ultimately exploring the complexity of novel inorganic molecules synthesized *via* non-traditional techniques such as low temperature electron irradiation of simple precursor ices.

Acknowledgements

The authors would like to thank the W. M. Keck Foundation (RIK) and the University of Hawaii (AMT, MJA) for support. Computer resources at the National Center for High-Performance Computing of Taiwan were utilized in the calculations.

References

- 1 I. Langmuir, *Proc. Natl. Acad. Sci. U. S. A.*, 1919, **5**, 252–259.
- 2 D. S. Parker, A. V. Wilson, R. I. Kaiser, T. Labrador and A. M. Mebel, *J. Am. Chem. Soc.*, 2012, **134**, 13896–13901.
- 3 D. Parker, A. Mebel and R. Kaiser, *Chem. Soc. Rev.*, 2014, **43**, 2701–2713.
- 4 C. E. S. Housecroft and A. G. Sharpe, *Inorganic Chemistry*, Pearson Limited, Harlow, UK, 2nd edn, 2005.
- 5 C. L. Berthollet, *Mem. Acad. Sci.*, 1785, **99**, 319.
- 6 P. Gengembre, *Hist. Mem. Acad. Roy. Sci.*, 1785, **10**, 651.
- 7 P. Thenard, *Acad. Sci. Paris*, 1844, **18**, 652.
- 8 C. A. L. de Bruyn, *Recl. Trav. Chim. Pays-Bas*, 1895, **14**, 85–88.
- 9 Y. Kim, J. W. Gilje and K. Seff, *J. Am. Chem. Soc.*, 1977, **99**, 7057–7059.
- 10 T. Fujii, C. P. Selvin, M. Sablier and K. Iwase, *J. Phys. Chem. A*, 2002, **106**, 3102–3105.
- 11 M. Baudler and K. Glinka, *Chem. Rev.*, 1994, **94**, 1273–1297.
- 12 M. Baudler and L. Schmidt, *Naturwissenschaften*, 1957, **44**, 488.
- 13 M. Baudler, H. Ständeke, M. Borgardt and H. Strabel, *Naturwissenschaften*, 1965, **52**, 345.
- 14 J. F. Shackelford and W. Alexander, *CRC Materials Science and Engineering Handbook*, CRC press, 2000.
- 15 B. M. Jones and R. I. Kaiser, *J. Phys. Chem. Lett.*, 2013, 1965–1971, DOI: 10.1021/jz400692r.
- 16 C. J. Bennett, S. J. Brotton, B. M. Jones, A. K. Misra, S. K. Sharma and R. I. Kaiser, *Anal. Chem.*, 2013, **85**, 5659–5665.
- 17 B. M. Jones, R. I. Kaiser and G. Strazzulla, *Astrophys. J.*, 2014, **781**, 85.
- 18 R. I. Kaiser, S. Maity and B. M. Jones, *Phys. Chem. Chem. Phys.*, 2014, **16**, 3399–3424.
- 19 B. M. Jones, R. I. Kaiser and G. Strazzulla, *Astrophys. J.*, 2014, **788**, 170.
- 20 S. Maity, R. I. Kaiser and B. M. Jones, *Faraday Discuss.*, 2014, **168**, 485–516.
- 21 R. I. Kaiser, S. Maity and B. M. Jones, *Angew. Chem., Int. Ed.*, 2015, **54**, 195–200.
- 22 S. Maity, R. I. Kaiser and B. M. Jones, *Phys. Chem. Chem. Phys.*, 2015, **17**, 3081–3114.
- 23 P. Maksyutenko, L. G. Muzangwa, B. M. Jones and R. I. Kaiser, *Phys. Chem. Chem. Phys.*, 2015, **17**, 7514–7527.
- 24 S. Maity, R. Kaiser and B. M. Jones, *Astrophys. J.*, 2014, **789**, 36.
- 25 D. Fulvio, B. Sivaraman, G. Baratta, M. Palumbo and N. Mason, *Spectrochim. Acta, Part A*, 2009, **72**, 1007–1013.
- 26 D. Hudgins, S. Sandford, L. Allamandola and A. Tielens, *Astrophys. J., Suppl. Ser.*, 1993, **86**, 713–870.
- 27 M. Westley, G. Baratta and R. Baragiola, *J. Chem. Phys.*, 1998, **108**, 3321–3326.
- 28 R. Brunetto, G. Caniglia, G. Baratta and M. Palumbo, *Astrophys. J.*, 2008, **686**, 1480.
- 29 P. Hovington, D. Drouin and R. Gauvin, *Scanning*, 1997, **19**, 1–14.
- 30 M. D. Francia and E. R. Nixon, *J. Chem. Phys.*, 1973, **58**, 1061–1065.
- 31 W. A. VonDrasek, S. Okajima and J. P. Hessler, *Appl. Opt.*, 1988, **27**, 4057–4061.
- 32 A. D. Becke, *J. Chem. Phys.*, 1992, **96**, 2155–2160.
- 33 A. D. Becke, *J. Chem. Phys.*, 1992, **97**, 9173–9177.
- 34 A. D. Becke, *J. Chem. Phys.*, 1993, **98**, 5648–5652.
- 35 C. Lee, W. Yang and R. G. Parr, *Phys. Rev. B: Condens. Matter Mater. Phys.*, 1988, **37**, 785.
- 36 G. D. Purvis III and R. J. Bartlett, *J. Chem. Phys.*, 1982, **76**, 1910–1918.
- 37 C. Hampel, K. A. Peterson and H.-J. Werner, *Chem. Phys. Lett.*, 1992, **190**, 1–12.
- 38 P. J. Knowles, C. Hampel and H. J. Werner, *J. Chem. Phys.*, 1993, **99**, 5219–5227.
- 39 M. J. Deegan and P. J. Knowles, *Chem. Phys. Lett.*, 1994, **227**, 321–326.
- 40 R. I. Kaiser, B. J. Sun, H. M. Lin, A. H. Chang, A. M. Mebel, O. Kostko and M. Ahmed, *Astrophys. J.*, 2010, **719**, 1884.
- 41 O. Kostko, J. Zhou, B. J. Sun, J. S. Lie, A. H. Chang, R. I. Kaiser and M. Ahmed, *Astrophys. J.*, 2010, **717**, 674.
- 42 M. J. Frisch, *GAUSSIAN 09, Revision D.01*, Gaussian, Inc., Wallingford CT, 2013.
- 43 J. Durig, Z. Shen and W. Zhao, *THEOCHEM*, 1996, **375**, 95–104.
- 44 F. J. Ding and L. F. Zhang, *THEOCHEM*, 1996, **369**, 167–172.
- 45 GRAMS/AI-Spectroscopy-Software, *Journal*, 2002.
- 46 J. Berkowitz, L. Curtiss, S. Gibson, J. Greene, G. Hillhouse and J. Pople, *J. Chem. Phys.*, 1986, **84**, 375–384.
- 47 S. Elbel, H. Tom Dieck, G. Becker and W. Ensslin, *Inorg. Chem.*, 1976, **15**, 1235–1238.
- 48 T. Fehlner, *J. Am. Chem. Soc.*, 1968, **90**, 6062–6066.
- 49 R. Haring, A. Haring, F. Klein, A. Kummel and A. De Vries, *Nucl. Instrum. Methods Phys. Res.*, 1983, **211**, 529–533.
- 50 A. De Vries, R. Haring, A. Haring, F. Klein, A. Kummel and F. Saris, *J. Phys. Chem.*, 1984, **88**, 4510–4512.
- 51 P. Gerakines, W. Schutte and P. Ehrenfreund, *Astron. Astrophys.*, 1996, **312**, 289–305.
- 52 L. Farenzena, P. Iza, R. Martinez, F. Fernandez-Lima, E. S. Duarte, G. Faraudo, C. Ponciano, M. Homem, A. N. de Brito and K. Wien, *Earth, Moon, Planets*, 2005, **97**, 311–329.
- 53 W. Zheng, D. Jewitt, Y. Osamura and R. I. Kaiser, *Astrophys. J.*, 2008, **674**, 1242.
- 54 H. B. Schlegel and A. Skancke, *J. Am. Chem. Soc.*, 1993, **115**, 7465–7471.
- 55 R. Hilbig and R. Wallenstein, *Appl. Opt.*, 1982, **21**, 913–917.